Development of Bio-Impedance Micro Probes for Integration with Smart Biopsy Tool

Vivek Jayabalan

Thesis submitted to the Faculty of the
Virginia Polytechnic Institute and State University
in partial fulfillment of the requirements for the degree of

Master of Science
in
Mechanical Engineering

Roop L Mahajan, Chair
Rafael Davalos
Masoud Agah

September 29, 2014
Blacksburg, Virginia

Keywords: Bio-Impedance Micro Probes, Smart Biopsy tool, Cancer Cell Seeding, Prevention, Micro fabrication, Polyimide

Abstract

Development of Bio-Impedance Micro Probes for Integration with Smart Biopsy Tool

Vivek Jayabalan

Biopsy is a standard practice in the diagnosis and treatment of many cancers. Despite its integral role in cancer diagnosis, in some instances, the biopsy tool facilitates metastasis by transferring cancerous cells attached to its exterior into the healthy tissue or the blood circulation during its retraction from the tumor. These few cancer cells can then serve as seeds for the malignant tumor to grow in the healthy tissue. Cauterization using extreme heat or cold can destroy cells in the region and minimize the chance of seeding but this can be an inexact process that increases damage to otherwise healthy tissue and prolongs healing time following a biopsy procedure.

In our laboratory, we have developed the concept of a new smart biopsy tool that can reduce the chance of cancer cell dissemination during a biopsy. This tool improves on the conventional biopsy needle by introducing an impedance sensor on the biopsy tool which is housed in a sliding sheath. Due to the significant difference in the electrical conductivity of the tumor and the healthy tissue, the sensor is able to distinguish between the two and locate the exact tumor interface. The protective sheath placed around the instrumented biopsy tool and above the interface isolates the healthy tissue and prevents or at least minimizes the

transfer of tumor cells. Delivering an RF dose through the sheath can kill any malignant cells that might be lurking around the interface. Figure 1, below, demonstrate a schematic of this envisioned device.

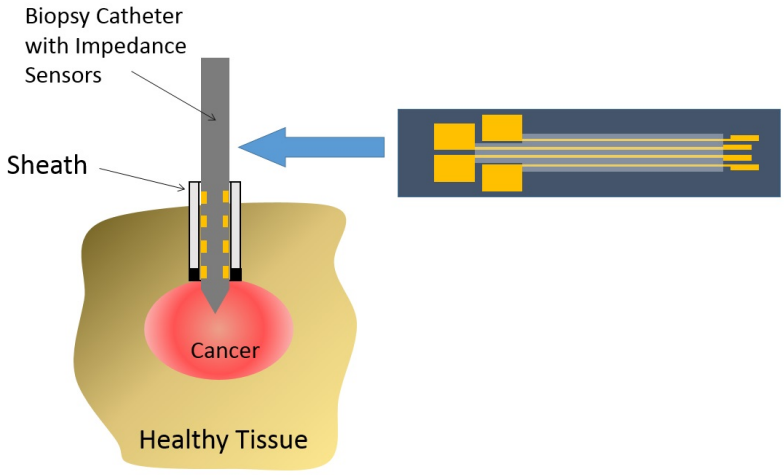

Figure 1: Schematic working of the smart biopsy tool showing the bio-impedance sensor

This thesis, in particular, will concentrate on the development of the design, fabrication and calibration of the impedance sensor and its integration with the biopsy tool. The impedance sensor essentially consists of conductive electrodes sandwiched between insulating layers. They are built on thin-film polymer, Polyimide, using conventional microfabrication techniques. These sensors are further calibrated to estimate the cell constant. Once calibrated, these probes are used to measure the conductivity of porcine tissues, and in-house prepared agar phantoms.

Acknowledgments

First and foremost I would like to offer my sincere gratitude to my advisor, Prof. Roop L Mahajan, who has supported me throughout this thesis with immense patience and knowledge, whilst allowing me the room to work in my own way. His passion and motivation moves one and all in ICTAS, and, I find myself very fortunate to have had the opportunity to work with him for over a year. With his heavily loaded schedule, Prof Mahajan always made time to make sure I was on the right track. Thank you sir!

I would like to thank Prof. Davalos, for introducing me to this project and to Prof. Mahajan. All of the work was done in lab facilities and I would like to thank him for graciously allowing me to use the space. He is the reason why I find myself belonging to this university. His class on Biomedical Microdevices, is one of the most interesting, inter-disciplinary classes I have had at Virginia Tech, and it convinced me to pursue interdisciplinary research for my degree here.

I have had the opportunity to collaborate with many extraordinary people. A special thanks to Mohammad Bonakdar, my friend, my colleague and my go-to person every time something was wrong, both academically and otherwise. His support, and his ideas have helped me deeply in this work and in my Masters Degree here. Special thanks to Lisa and Sai, with whom I had collaborated two projects for the course work of MEMS and Biomedical Microdevices.

The tissue test results are a very integral part of my thesis and it would have been impossible without the help from the wonderful people at Vasowave lab. My sincere thanks to Prof. John Robertson, for making me the space to perform my experiments. My thanks to Chip Aardema Jr and Tim O'Brien, who helped me procure and handle the tissue. I would also like to express my gratitude to Steve Mc Cartney, of NCFL, ICTAS II, for helping me image my probes in Scanning Electron Microscope. My sincere gratitude to Dr. Masoud Agah, for advising me on how I might be able to use wire bonding and his course, MEMS: Fabrication to Application, which built and strengthened the fundamentals I needed to work on my thesis.

It has been an adventure travelling half-way around the world. To all my wonderful friends here, at Blacksburg, and in US, without whom it would have been impossible to survive. Special thanks to Abhishek, Sudarshan Aji, Vineeth and Vishnu, to have looked out for me, and for having sat through all my whining.

To my parents, I want to express my deepest gratitude. Words can do little justice to the great deal of sacrifice they have gone through over the two years, just so that I could pursue my dream. I am more the indebted, and in a little-big way, blessed!

Amma and Appa, I would like to dedicate this thesis to you both.

Contents

List of Figures

List of Tables

Chapter 1

Introduction

Fine needle aspiration Biopsy (FNAB) is the first procedure of choice in Europe, large parts of Asia and in most academic centers of US, and is the decisive diagnostic procedure before any drastic cancer therapy begins.

Recent developments in the field of diagnostic radiology have introduced tools like computerized tomography, digital vascular imaging, and NMR. These advances have improved non-invasive cancer diagnostics but havent replaced the conventional biopsy-based tissue verification [1]. This is mainly due to the high diagnostic specificity and sensitivity of cytological verifications as compared to those with the other non-invasive cancer diagnostics. Thus, percutaneous needle biopsies, which are often heralded for their simplicity, speed, and low cost, continue to be the technique of choice and are performed more than ever before [2]. This has led to a number of studies with detailed discussions that critique the apparent safety and have carefully quantified the many associated risks [2–4]

Richard Terry [2] reviewed over 10,600 reported cases of biopsies performed on the liver. The study demonstrated that patients who underwent biopsy suffered from complications such as hemorrhage, biliary peritonitis, penetration of abdominal viscera, and tumor seeding. He reported a mortality rate of 0.12% and a complication rate of 0.32%. The major cause of

death was hemorrhage. However, it is quite likely that these deaths were caused by underlying disorders, like cholangiolitic hepatitis, congestive heart failure with hepatosplenomegaly, Hodgkin's disease, and Weil's disease. Similarly, this review notes that the biliary peritonitis complication is to be assessed in relation to patients with jaundice rather than with the liver biopsy itself. With an exception of needle-tract seeding, almost all other complications listed in this review seems to have an underlying patient condition, which cannot be dismissed or attributed to the procedure alone.

Livraghi et al., [3] reviewed 11,700 cases of fine-needle abdominal biopsies, among which 6 patients suffered from major complications and 24 patients with less severe complications. Among the 6 major complications, 2 patients suffered from needle-tract seeding. Other causes included one case each of intrahepatic hematoma, peritonitis after abscess puncture, and two cases of bile peritonitis.

While most of these complications involve other parameters and, are often, very case specific, one common complication that seems to accompany any biopsy procedure is the cancer cell seeding/metastases along the needle tract. The subsequent part of this thesis, will involve understanding and addressing this problem and proposing a solution for it.

1.1 Cancer Cell Seeding

A semi-quantitative lab study, by Ryd et al., [4] which performed fine needle biopsies on solid or ascites-growing mouse tumors demonstrated that one can seed about 10^3 – 10^4 cells during the procedure. This study was done under lab specifications using strictly inbred mice with extremely cellular and dedifferentiated tumor cells syngeneic with the host. They subsequently concluded that this risk translates rarely in clinical conditions and in human neoplasia, but for highly malignant tumors it was advised to remove the needle tract, wherever possible.

Needle-tract seeding poses a peculiar problem; several reviews have scrutinized the evidence of tumor spreading along the needle tract, and concluded that such metastases pose significant danger. There can be complications to this problem, especially when the neoplasia can intravasate in blood stream and/or the lymphatic system. [5]

It is difficult to quantify a specific risk for a problem involving several parameters. The risk of needle track seeding or cell displacement can be very case specific, device dependent and often is very organ sensitive. Many reviews and prospective studies provide only estimates of incidence rates amongst the included cases. In one of the reviews that studied complications in percutaneous abdominal fine needle biopsy, it was estimated that needle-tract seeding had a mortality rate of 4 out of the 63,108 cases studied, which attributes to a very small 0.005% incidence rate [6]. A review in studying hepatocellular cancer demonstrates such a rate of 2.7% overall and about 0.9% per year [7], whereas a review of pleural mesothelioma demonstrates the mean incidence of malignant seeding being about 19%. Subsequent papers have indicated extreme incidence rates between 2% to 51% [8]

Knight et al., [9] made an observation where the comparison of needle track seeding had little effect, between Image-Guided Core Needle Biopsy (IGCNB) and Needle Localization Breast Biopsy (NLBB). Of the 398 studied cases, 297 patients underwent IGCNB and 101 Patients underwent NLBB. Of these, 15 Patients demonstrated local recurrence with 11 of them having undergone IGCNB (3.7%) and 4 patients NLBB (3.96%).

Table 1.1: Incidence rate of Needle-Tract seeding in various conditions

Type of Cancer or Organ studied	Seeding reported	Number of Cases	Years	Country	Other Comments
Hepatocellular Cancer	2.7% Overall, 0.9% per year	NA (Review of other reviews)	Up to 2007	United Kingdom	[5]
Pleural Mesothelioma	40% Untreated, 0% Treated	20	1995	France	Effect of Radiotherapy on metastases of secondary tumor at the entry sites of thoracoscopy trocars or chest tubes, and/or cytology or biopsy needle
Mouse Tumors	$10^3 - 10^4$	NA	1983	Sweden	Demonstrates that the FNAB is a safe technique. The study used extremely cellular and malignant tumor lines, and it was proved about 1000-10000 cells could be implanted along the needle tract [4]
Breast Cancer	3.70%	398	2002	USA	Comparison of IGCNB v/s NLBB [9]
Breast Cancer	11 Cases of Tumor Cell displacement	64	2004	Netherlands	Histological studies of patients with excision on the same

The Table 1.1 demonstrates the risk of needle tract seeding under various discussed conditions. Most of these papers demonstrated a low incidence rate; the generic tone of these reviews is to dismiss any fears against employing these diagnostic procedures. A general conclusion is that the risk of not employing these diagnostic tools is far higher and lethal. Subsequent local radiotherapy has proven to counter any such metastases. However, not being able to deliver local radiotherapies for any medical reason poses a potential risk. This needs to be addressed by developing better biopsy techniques.

1.2 Prior work in the prevention of the Cancer cell seeding

Case studies and reviews discussed previously have established that cancer cell seeding along the needle tract is a serious complication and can possibly risk patients life. However, detailed literature search demonstrates that there has been little work done in this domain.

The common procedure, currently followed, is for the patient to undergo a local radiotherapy post a positive diagnosis. A randomized prospective study [8] assessed the efficacy of this therapy. Their study included 40 patients with pleural mesothelioma. These patients had a life expectancy of over 3 months at the time of diagnosis. Forty patients were divided into two groups of 20 each, where the first group underwent local radiotherapy and the latter did not. It was seen that the patients who were administered with local radio therapy did not develop any subcutaneous nodules. Eight patients out of the other 20 developed subcutaneous nodules, at the entry sites of the biopsy needles and/or thoracoscopic trocars. This work concluded by saying that the local radiotherapy irradiation is a safe and an effective technique to remove any seeded tumor cells. The study also suggested an optimum delay period to irradiate the seeded cells after the healing of the thoracoscopic scar or the needle scar to be 10–15 days. This narrow window also poses certain concerns, especially if

the patient is not medically ready, or misses this window over other medical and nonmedical reasons

More recently, ideas around manipulating biopsy tools to prevent the cancer contamination along the needle tract have been developed. Woitzik et al., [10] presented a polyethylene sheath device that reduces the risk of cell-spread during the biopsy procedure. Their device was a conventional biopsy tool with a 5µm think polyethylene sheets covering the cannula. When the biopsy needle is withdrawn, the polyethylene sheath prevents the contamination, after which the sheath itself is removed. However, their work also notes that while this technique reduces the risk of cancer spreading, the technique needs to be optimized.

Ivorra [11] developed an electrochemical way of preventing needle-tract seeding. He proposed to create a toxic environment around the biopsy needle using electrochemical techniques to prevent the cancer cell dissemination. By infusing DC currents, the biopsy needle acts as a cathode, while the tissue surrounding acts as the electrolyte of an electrolytic cell. With careful numerical simulation, the extent of toxic environment could be estimated and, thus, contained, there-in creating a small opening through which the needle can be removed with a reduced risk on cell dissemination. While this work has substantial numerical calculations and is an interesting engineering solution, little has been done to develop such a tool into an active replacement for the conventional biopsy procedure. Possible risks, such as allergies, skin sensitivity etc. have not been analyzed. The author also notes possible subsequent damage by joule heating and undesirable neuromuscular stimulations.

A more recent work by Feng et al. [12] proposed using a two-step freezing after a lung cancer biopsy. This innovative technique was performed on a 72 year old man who was diagnosed with a large mass in right upper lobe. The authors describe that the risk of spreading can cause a potentially resectable tumor to become unresectable. The procedure involved a two-step freezing method by imaging-guided percutaneous cryoablation, around the biopsy sheath, to prevent cell dissemination during the tool withdrawal. Figure 1.1 shows the

cryoablation of the tumor. This work is interesting, however, this technique leaves a ball of central tissue necrosis whose radius is about 3cm. This work may be very case-sensitive and may not be viable for other cancer lesions. It was also indicated that the Imaging-guided cryoablation has an acceptable complication rate.

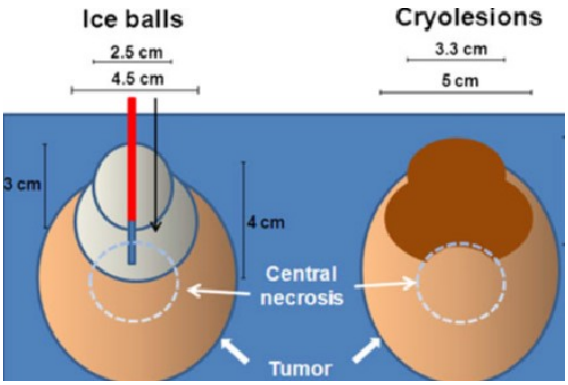

Figure 1.1: Representative schematic indicating the central necrosis in the two-step freezing technique. F. Mu, S. P. Liu, X. L. Zhou, J. B. Chen, H. B. Li, J. S. Zuo, and K. C. Xu, "Prevention of needle-tract seeding by two-step freezing after lung cancer biopsy", *Pathology & Oncology Research*, vol. 19, no. 3, pp. 447–450, 2013. Used under fair use, 2014.

1.3 Smart Biopsy Tool, to prevent needle tract malignant seeding

The current technologies are limited when it comes to preventing the seeding of malignant cells along the needle-tract. The developments, as discussed previously, are either very case-specific or are far from being a commercial product to replace conventional biopsy. Techniques like the electrochemical way of prevention, presented by Ivorra et al., [11] will need to be approved as a safe diagnostic technique from a regulatory authority like FDA, as it is substantially complicated and would need special training before the tool can be used.

Thus, solution needs to be engineered that does not drastically modify the conventional biopsy needles but yet can reduce the risk of cancer cell dissemination, and replace most

common biopsy procedures.

On these lines we propose a smart biopsy tool which can locate the interface between the pathological and healthy tissues and prevent the cell dissemination along the needle-tract. This tool improves on the conventional biopsy needle by introducing an impedance sensor on the biopsy tool which is housed in a sliding sheath. Figure 1.2 shows the representative sketch of this tool.

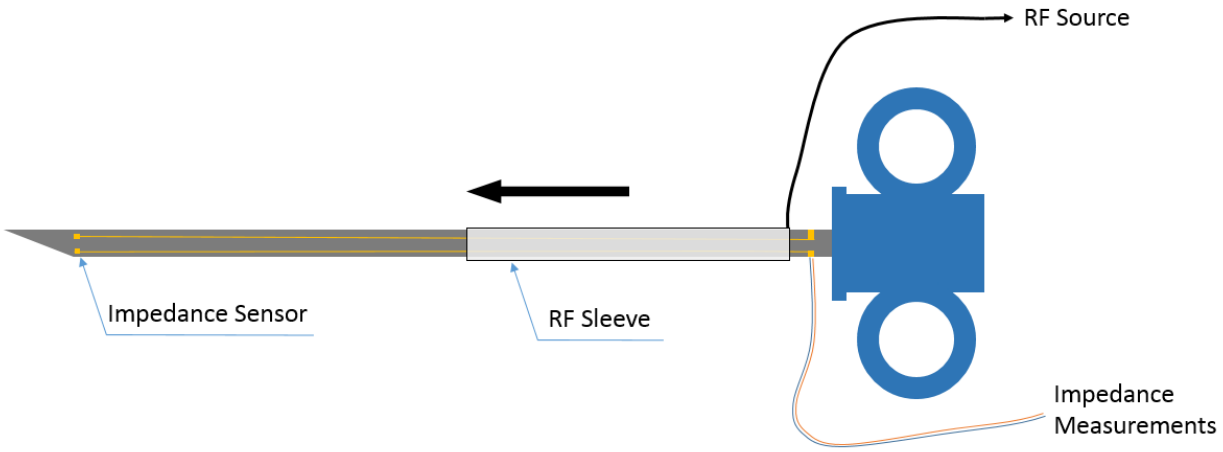

Figure 1.2: A representative sketch of the proposed smart biopsy tool. The black arrow indicates that the sleeve can be moved during the procedure

During the biopsy, with the help of the impedance sensors, one can actively monitor the in-vivo impedance of the tissue. With the significant difference in the electrical conductivity of the tumor and the healthy tissue, the sensor can distinguish between the two and locate the exact tumor interface. At this interface the protective sheath is inserted, and placed around the biopsy needle, isolating the healthy tissue from the tumor there by reducing the chance of any tumor cell transfer. Once the required biopsy is performed, the region is doused with RF energy with the help of the inserted sheath, and killing any malignant cells that might be lurking around the interface. Figure 1.3 demonstrates the working of the smart biopsy tool.

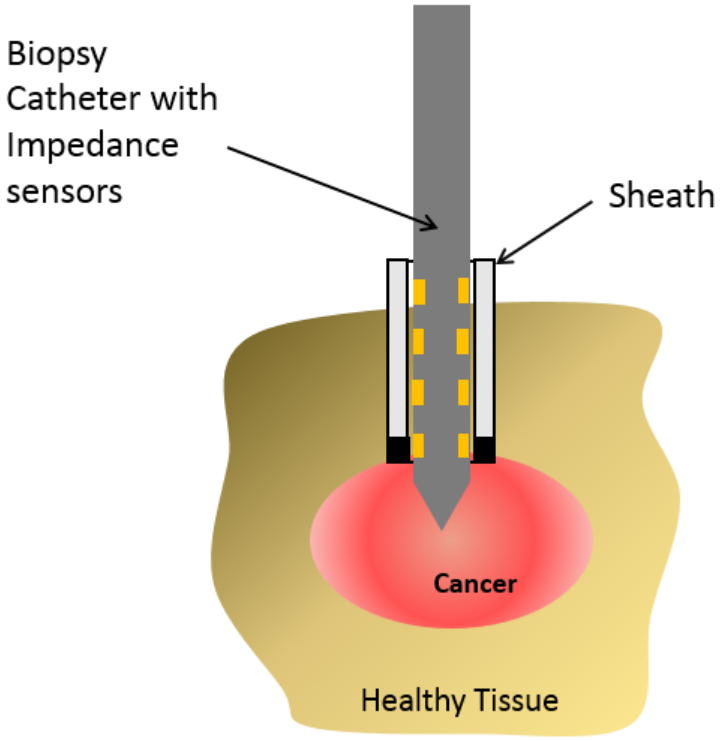

Figure 1.3: Schematic working of the tool

The positioning of the sleeve during this procedure is extremely crucial and must be positioned exactly at the interface of regular tissue and the tumor. Most biopsy today are guided using ultrasound, while the precision of this imaging technique is substantially accurate for extracting tissue, it may be little of for positioning the RF Sleeve. This necessitates a bio-compatible impedance sensor that can be integrated with the needle itself. Commonly noted difference in the malignant tumors and regular tissue is its impedance. The following section discusses the difference between the bio-impedance of various cancer tumors and regular tissues. [13]

1.4 Bio-Impedance of Cancerous Tissues

As early as in 1920, Fricke and Morse [14] established the significant difference of capacitance between malignant breast tumors and normal tissue. Since then there have been substantial studies demonstrating that malignant tumors, breast and otherwise, have significantly higher impedivity than regular tissues.

In one of the earlier seminal studies, Smith et al. [15] demonstrated that the in-vitro conductivity of liver carcinoma from 1 kHz to 13MHz was about 6–7.5 times higher than of regular tissues. Schepps and Foster [16] established that the differences in the conductivities between normal and tumor tissues in the microwave frequency range stems primarily due to the difference in the water content in these cells.

Morimoto et al., [17] were the first to report results of human in-vivo measurements for breast and pulmonary carcinomas in the radio-frequency range. They concluded that the three parameters studied, extracellular resistance, intracellular fluid resistance, and cell membrane capacitance, exhibit significant differences between various tissues and tumors; suggesting possible diagnostic applications.

Haemmerich et al., in 2003 [18] measured in vivo electrical properties of hepatic malignant tumors and normal tissues in a frequency range of 10 Hz to 1 MHz, and at different tumor stages between 6 and 12 weeks after induction. The results demonstrated a significant difference between normal and tumor tissues. At 10 Hz normal liver tissues measured 1.26 $\pm$ 0.15 $\mathrm{mScm^{-1}}$, while tumor measured 2.69 $\pm$ 0.91 $\mathrm{mScm^{-1}}$. Similarly in the other end of spectrum the tissue conductivity measured was 4.61 $\pm$ 0.42 $\mathrm{mScm^{-1}}$, and the tumor conductivity was 5.23 $\pm$ 0.82 $\mathrm{mScm^{-1}}$.

Most of the measurement done in the literature above are performed using cylindrical electrodes placed around the tissue, thus measuring a 'global' value particular to that tissue.

However, the impedance sensor we intend to employ shall measure the average impedance of a small area of tissue surrounding the biopsy needle. Furthermore, during the biopsy procedure the tissue is locally ripped increasing the blood flow in this region thereby increasing the conductivities of that region. Thus, while using our device we may not be able to exactly corroborate to the conductivity reported in the literature, however, our motivation to introduce this impedance sensor is to identify the tissue-tumor interface. The impedance sensor will watch for a spike in the measured conductivities around the tumor region.

These reports are detailed enough to establish impedance tomography [19,20] as a diagnostic field in itself, and we intend to exploit this difference by introducing an impedance measurement sensor in the conventional biopsy needle as the first advancement in the development of the 'Smart biopsy tool'.

1.5 Outline of this thesis

Engineering the smart biopsy tool discussed above consists of two distinct components: the RF sleeve, and the bio-impedance sensor. This thesis, will focus on the design, fabrication and integration of the impedance sensor with the biopsy needle. Figure 1.4 shows the fabricated bio-impedance sensor, which can be integrated with the biopsy catheter

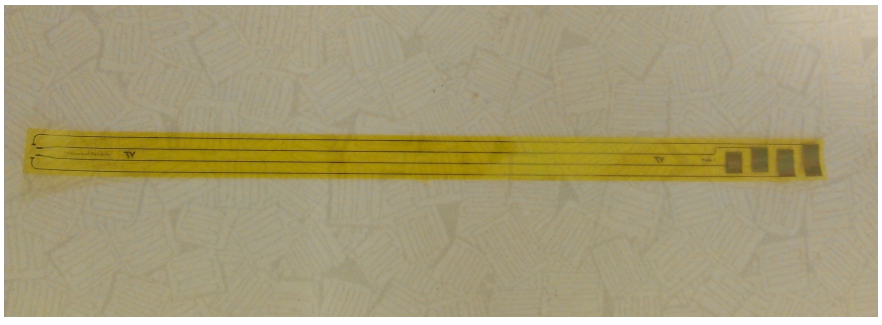

Figure 1.4: Fabricated bio-impedance sensor

The following chapter presents a mathematical modelling of the two kinds of impedance

sensors—the two-electrode probes and the four-electrode probes. It is followed by a detailed description of the fabrication technique involved including difficulties experienced and solutions to overcome these.

The third chapter in this thesis will present the calibrations of the fabricated probes using standard salt solutions and demonstrate their viability to measure tissue conductance using agarose gel phantoms. The final chapter will provide the summary and the conclusion of this project, and demonstrate the scope for future work and analysis.

Chapter 2

Modelling and Fabrication of Bio-impedance Microprobes

The previous chapter introduced the problem of cancer cell dissemination during biopsy procedures and established the need for a smart biopsy tool to prevent such complications. The biopsy tool comprises of a RF sleeve which when placed at the interface of the tissue-tumor ablates the displaced cells. The sleeve is to be placed exactly at the tissue-tumor interface by the help of an impedance sensor on the biopsy tool. The impedance sensor exploits the inherent difference of conductivities between the tissue cells and the cancer cells, as discussed in Section 1.4

This impedance sensor needs to be small, thin, have a linear response for changing conductivity in its media, and be flexible to be mounted around the needle. It is also important that the sensor materials will not set-off allergic reactions inside a human body. Most polymers dont cause allergic reactions and are often employed in medical instruments. Thin-film polymers, like polyimide, are very strong and flexible, and can be easily wrapped around the needle. Thus, these sensors are fabricated using conventional MEMS fabrication techniques on thin polyimide films. Their fabrication is discussed later in this chapter

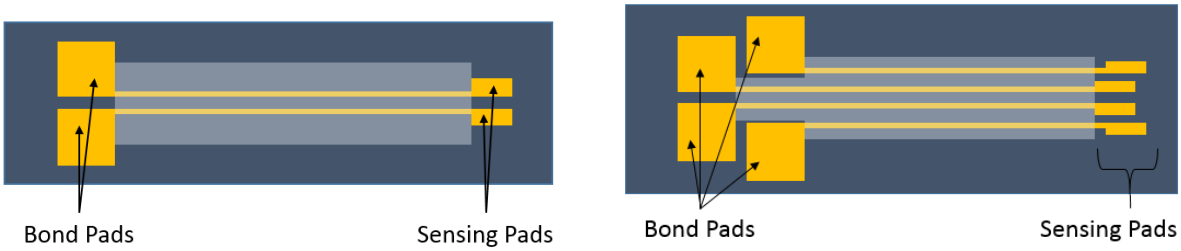

(a) Two electrode probe (b) Four Electrode Probe

Figure 2.1: A representative sketch of the electrode probes

Commonly used bio-impedance sensors are either bi-polar or tetra-polar. As the name suggests, bi-polar impedance sensors have two electrodes across which the current flow is measured. Tetra-polar sensors have four electrodes, two of which are used to inject current and the other two are employed to measure the voltage drop. It is commonly argued that the tetra-polar sensors are more reliable and have better signal-to-noise ratios. Figures 2.1a and 2.1b are representative pictures of the two probes

These sensors, once fabricated, measure conductance when introduced in a medium of particular conductivity. With an increase in the conductivity of the media, the probes demonstrate higher conductance. The relationship between the conductivity and the conductance is linear and is scaled by a constant called the cell-constant. Theoretical definition of the cell constant for these probes are discussed below

2.1 Theoretical cell constant for a two electrode probe

The cell constant 'κ' is the scaling constant between the specific conductivity 'σ' of the medium against the conductance '$\mathbb{C}$' measured by the probe, as shown in equation 2.1.

$$\sigma = \mathbb{C}\kappa \tag{2.1}$$

The inverse of equation 2.1 relates in the following way, where 'R' is the measured resistance and 'ρ' is the media's resitivity

$$R = \rho\kappa \tag{2.2}$$

Its known that for any two conductors of arbitrary shape separated by a dielectric medium of non-zero conductivity, the following expression, can be derived using Ohm's law and Maxwell's equation [21]

$$RC = \frac{\oiint \epsilon_0\epsilon_r E.ds}{\oiint \sigma ds} \tag{2.3}$$

The symbols represent conventional parameters: 'E' stands for the electric field, 'R' resistance, 'C' capacitance, 'ϵ_0' dielectric co-efficient of vacuum and σ is the conductivity of the media with a dielectric co-efficient of 'ϵ_r'. With the assumption of an isotropic media of a particular dielectric coefficient, the surface integrals of equation 2.3 can be evaluated and reduced to

$$RC = \frac{\epsilon_r\epsilon_0}{\sigma} \tag{2.4}$$

Combining equation 2.1 and 2.4, we get the expression for the cell constant as

$$\kappa = \epsilon_0\epsilon_r C \tag{2.5}$$

Thus, from equation 2.5, the theoretical cell constant of a particular set of probes can be estimated by determining their capacitance.

Capacitance of a pair of normally independent electrodes positioned side by side is a well-documented problem, and has been of interest since the advent of microelectronics [21]. Here, we use the expression published by Kaiser and Castro [22].

Consider a pair of two conductors as shown in figure 2.2a, with a width of l, Length L (in the outward normal to the plane of this paper) and separated by a distance d, and immersed in a dielectric medium of thickness t. The capacitance of this configuration can be evaluated using a conformal transformation to a pair of parallel plate conductors. The analytical expression for such transformations are derived using conformal mapping and are discussed as typical examples in most Electromagnetic theory books [21].

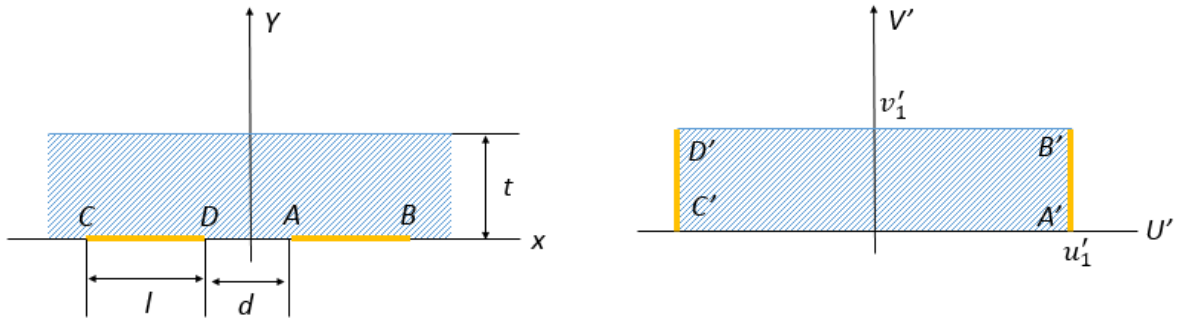

(a) Pair of conductors in a dielectric medium

(b) Transformation used by Kaiser and Castro to evaluate the conductivity

Figure 2.2: Representative sketch of conductors in dielectric medium

The evaluated capacitance of unit length from this method is [21]

$$C_L = \frac{C}{L} = \frac{\epsilon_0 \epsilon_r}{2} \left\{ \frac{F\left[\sqrt{1-\left(\frac{u_1}{u_2}\right)^2}, \frac{\pi}{2}\right]}{F\left[\frac{u_1}{u_2}, \frac{\pi}{2}\right]} \right\} \tag{2.6}$$

Here, $F[\alpha, \phi]$ is the incomplete elliptical integral of the first kind and the ratio $\frac{u_1}{u_2}$ is derived from the conformal mapping and is

$$\frac{u_1}{u_2} = \frac{1 + \tanh\left(\frac{\pi L}{2t}\right) \tanh\left(\frac{\pi d}{4t}\right)}{1 + \frac{\tanh\left(\frac{\pi L}{2t}\right)}{\tanh\left(\frac{\pi d}{4t}\right)}} \tag{2.7}$$

For our conductivity electrodes, where the width of the electrodes is in the order of few hundred microns and the thickness of the media which is being monitored is in the order of few centimeters, it is safe to assume that the thickness of the dielectric membrane is far higher than the dimensions of the probe. Thus with the following limits:

$$\eta = \lim_{t \to \infty} \left(\frac{u_1}{u_2}\right) = \frac{1}{1 + \frac{2l}{d}} \tag{2.8}$$

The cell constant for bi-polar probes can be reduced by combining equations 2.5, 2.6 and 2.8

$$\kappa = 2L \frac{F\left[\eta, \frac{\pi}{2}\right]}{F\left[\sqrt{1-\eta^2}, \frac{\pi}{2}\right]} \tag{2.9}$$

For any two rectangular co-planar conductors of length L, width l, and spacing d one can estimate the elliptical integrals, and subsequently the cell constant

2.2 Theoretical Cell Constant for Four Electrode Probes

The four-electrode technique is generally used for measuring tissue conductivity, or conductivities of anisotropic dielectric media. This technique employs four electrodes, with the current applied through the outer electrodes and the voltage measured across the inner electrode. Use of separate electrodes to measure the voltage prevents the problem of electrode polarization, thus having better signal to noise ratio.

Given an anisotropy similar to myocardial cells, where one can expect a conductivity along the myocardial fiber and another conductivity value when measured perpendicular to the direction of fibers, Steendijk et al. [23] in their paper demonstrated how with these probes, one can determine the conductivity values along and perpendicular to the fibers. Their method to calculate resistivities approximates the geometry and the electrical property of the medium under study as either 'infinite', 'semi-infinite' or 'thin'. Thus this method yields a result which is 'weighted spatial average' over a small domain. An 'infinite' region model is used when the probes are surrounded by the dielectric media, under observation, in all the direction. Whereas, a 'semi-infinite' region model is used when one of the sides of the sensory electrode has either an isulating membrane or doesn't have the di-electric media. Equation 2.10 shows the relation for an 'infinite' media, while equation 2.11 shows the relationship for a 'semi-infinite' media.

$$R_{inf} = \left(\frac{I}{4\pi a}\right)\rho \tag{2.10}$$

$$R_{sinf} = \left(\frac{I}{2\pi a}\right)\rho \tag{2.11}$$

The four electrode probe on the biopsy tool measuring the conductivity of the tissue is modeled with 'semi-infinite space'. Thus for an equally spaced four-electrode probe the measured voltage relates with the applied current as

$$V^{sinf}_{measured} = \left(\frac{I_{app}}{2\pi a}\right)\rho \tag{2.12}$$

where I_{app} is the applied current, a is the inter-electrode distance, and ρ is the conductivity inverse of the media. The equivalent cell constant derived from equation 2.12 is

$$\kappa = \frac{1}{2\pi a} \tag{2.13}$$

Suesserman et al. [24] in their paper on characterizing these probes, derived from first principles this expression in equation 2.12 and also demonstrated how the expression varies with changes in the array of the electrodes. For an array, where the distance between the inner electrodes in b, while the total length of the array being $2a + b$, the cell constant was shown to be

$$\kappa = \frac{1}{2\pi}\left(\frac{2b}{a(a+b)}\right) \tag{2.14}$$

Ideally larger κ value implies a better response for the change in the medias conductivity; thus a more sensitive probe. From equation 2.14 it is obvious that for higher κ, the ratio b/a needs to be as large as possible. This distance ratio named as the 'Inter-Electrode Separation Distance' or IESD by Ivorra et al. [25] is considered as the pivotal design consideration while fabricating these probes.

While large κ values improves the sensitivity of the device, it compromises the spatial resolution to identify medium transitions. Consider a situation as shown in figure 2.3 where the four electrode probe is placed close to an interface. The measured conductance at this place will be different from the material's conductance.

The expression for this measured conductance was analytically derived using the method of images by Robillard et al. [26]. He proposed that the ratio of the measured conductivity of

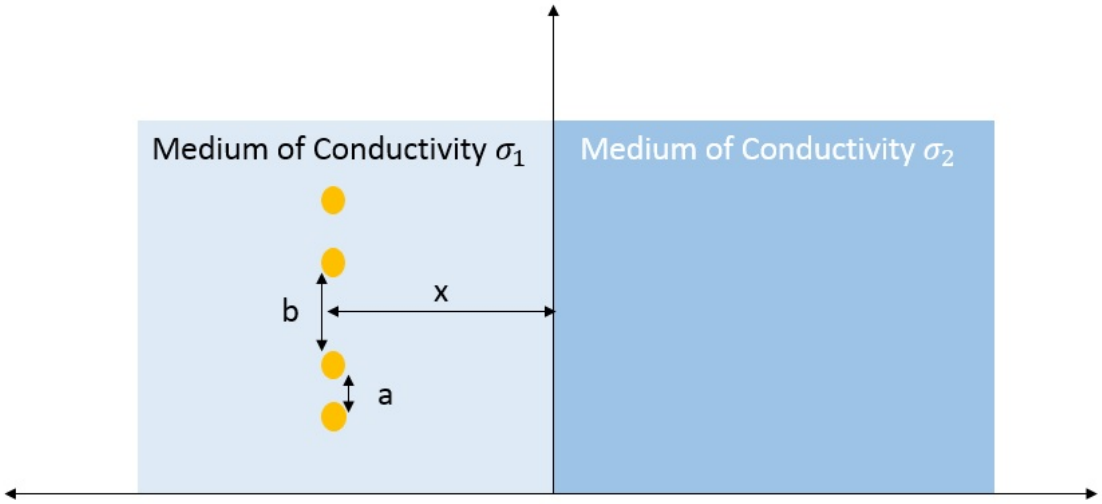

Figure 2.3: Schematic of a probe near a medium transition

the media (σ'), normalized against the media's conductivity (σ) is related to a perturbation term $\left(\frac{KG'}{G}\right)$ by the following equation

$$\frac{\sigma'}{\sigma} = \frac{1}{1 + K\left(\frac{G'}{G}\right)} \tag{2.15}$$

The term K is defined by the following relationship, where σ_1 and σ_2 are the conductivities of the two media as shown in the figure 2.3.

$$K = \frac{\sigma_2 - \sigma_1}{\sigma_1 + \sigma_2} \tag{2.16}$$

The spatial terms G' and G are defined in the equation 2.17 and 2.18

$$G' = \left[\frac{1}{\sqrt{4x^2 + a^2}}\right] - \left[\frac{1}{\sqrt{4x^2 + (a+b)^2}}\right] \tag{2.17}$$

$$G = \frac{1}{a} - \frac{1}{a+b} \tag{2.18}$$

where, x is the perpendicular distance of the probe from the media, and a and b are the inter-electrode separation as demonstrated in the figure 2.3. For a medium transition, where the conductivity of media are 3mS/cm and 15mS/cm, and a probe with a/b ratio of 2, the normalized spatial co-ordinate is plotted against the normalized measured conductivity. Normalized spatial co-ordinate is the distance x, as shown in figure 2.3, normalized against the inter electrode difference a as shown again in figure 2.3. Similarly, the normalized conductivity plotted, is the measured conductivity by the probe against the actual conductivity of the media. The transition occurs at $x/a = 0$. From the plot 2.4, it can be noted that the resolution of identifying the interface is approximately four times the inter-electrode distance a.

With these criteria in mind, the mask was carefully designed with various two and four electrode probes. Most probes in our design include an inter-electrode distance of between 200µm – 500µm, yielding a theoretical spatial resolution of not more than 2mm. The following section will detail some of the challenges faced during the fabrication of these probes.

2.3 Fabrication of the designed probes

As discussed previously, the probes to be fabricated must be manufactured on thin-film polymers that can be mounted around the biopsy needles. Majority of percutaneous biopsies are performed using needles, typically ranging from 16–21 gauge. Musculoskeletal biopsies are typically performed using needles ranging from 11–14 gauge [5]. Thus the probes can have a width between 2mm–4mm.

Developing probes that are about 4mm wide, with a high spatial resolution, and on thin film

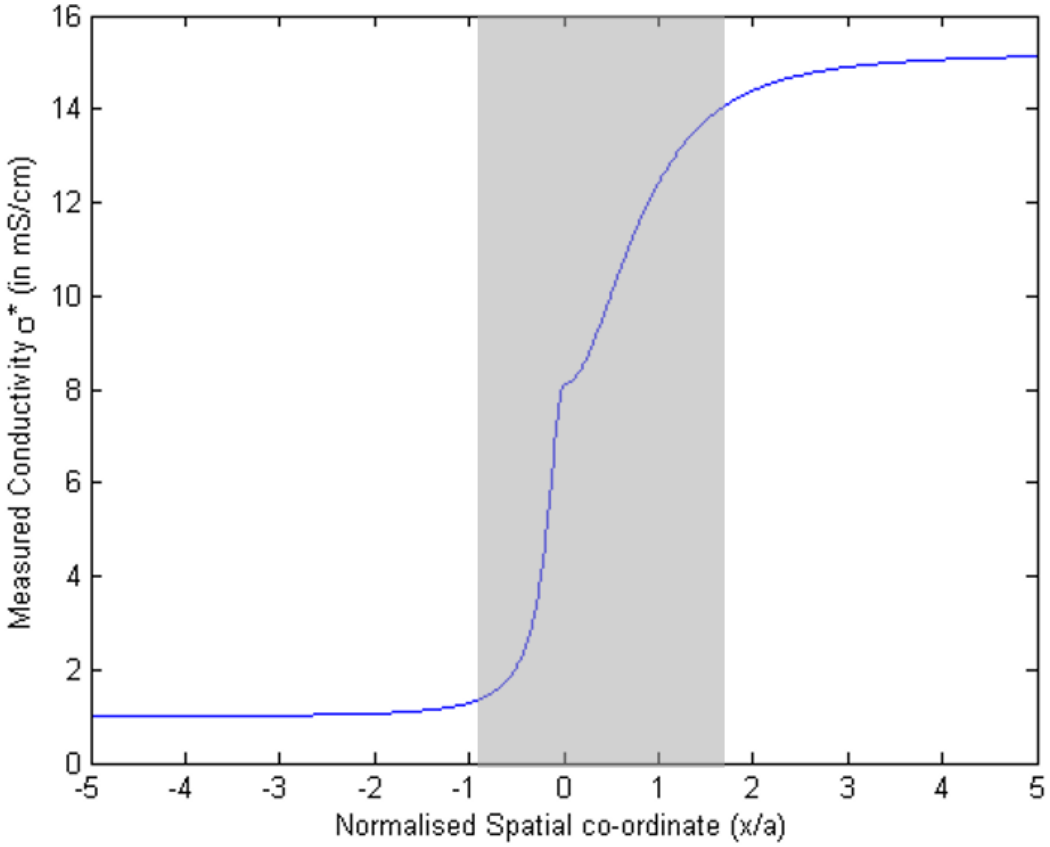

Figure 2.4: Effect of close medium transitions derived using the method of images

flexible polymers, can deploy conventional MEMS fabrication techniques. Such probes can be fabricated by sandwiching patterned conductive electrodes between insulating polymers. The conductive electrodes were decided to be gold, for its high conductivity and ease in patterning the material. Polyimide is a commonly used bio-compatible polymer with fairly easy patterning ability. Gold can be patterned using any common photo-resist as the mask. Polyimide, on the other hand, which is usually etched in RF Plasma etch, needs to have titanium as the masking layer.

With the above design constraints, the mask shown in figure 2.5 was developed. This mask had probes that are 4.5mm wide and had the conductive sensors region not wider than 1.7mm. The mask has 5 two electrode probes, and 10 four electrode probes with varying IESD. These probes where fabricated on typical 150mm silicon wafers. Commercial polyimide, PI2525, was used. This polymer was spun coat on the wafers followed by soft baking it on hot plate at 110°C. Gold and chrome were deposited on the wafer using PVD technique and patterned with the mask show above. The photoresist used was AZ9260. Gold/Chrome layers were etched to make the probes using the mask shown above.

The second layer of polyimide was then spun and hard baked at 200°C for 30 minutes and subsequently, at 300°C for 1 hour in a nitrogen media. This baking process was done with slow ramps of 5°C/min. Once cooled down, with a similar ramp, the wafer was set for the PVD of titanium. The titanium acts as a mask for etching the polyimide in oxygen plasma.

Initially, each layer of polyimide was etched individually. Once the top layer of polyimide was etched, Ti was deposited again to mask the exposed bottom layer of the polyimide inside the probe region. The second layer of Ti was patterned and the bottom layer of polyimide was etched. As the final step, the titanium was removed by dousing the wafer in buffered oxide etch for less than a minute. This automatically released the probes from the wafer. Figure 2.6 shows the released probe that can be subsequently integrated with biopsy catheters This process, while sounds good in theory, had issues. The etch rate of polyimide in plasma around the exposed conductor was much higher than the etch rates at other places. This substantially weakened the bottom polyimide around the bond pads in particular. Figure 2.7 shows the tear near the bond pads that almost always occurred when using this process.

This problem prompted a change in the fabrication process. It was proposed to change the insulating layer by using either silicon di-oxide or silicon nitride as the insulating membrane over Polyimide. However, the leakage current when using chemically vapor deposited SiO_2,

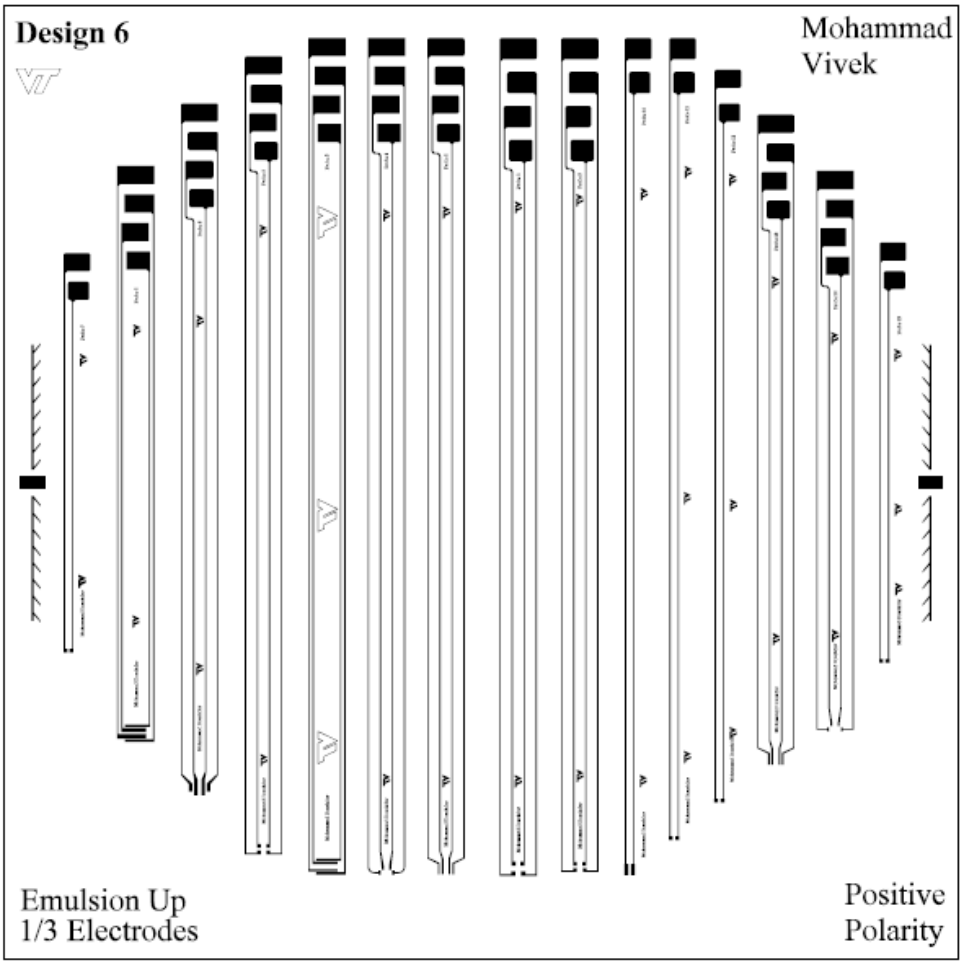

Figure 2.5: Preliminary mask showing the conductive probes

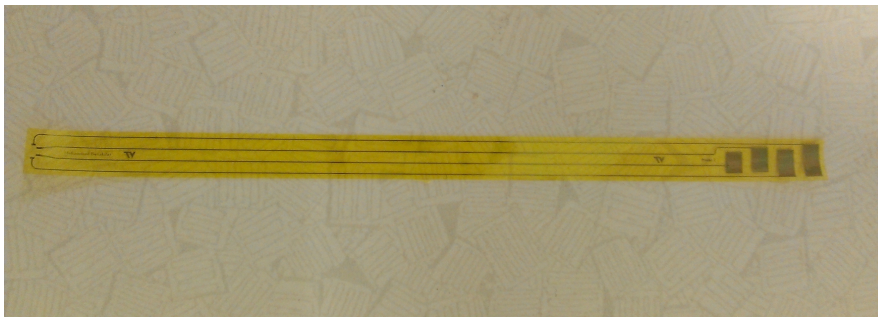

Figure 2.6: Fabricated bio-impedance sensor that is to be integrated with the biopsy needle

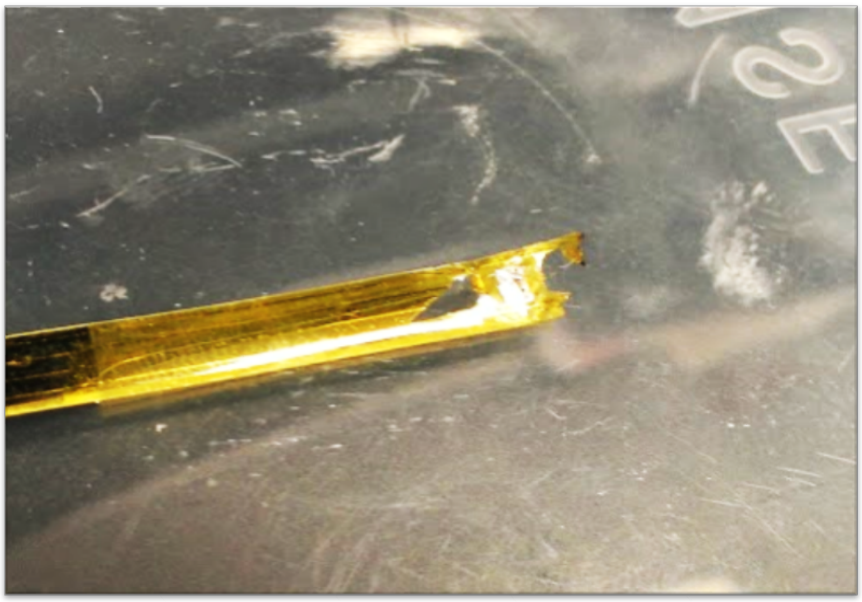

Figure 2.7: High etch rates of the polyimide around the bond-pads make them weak

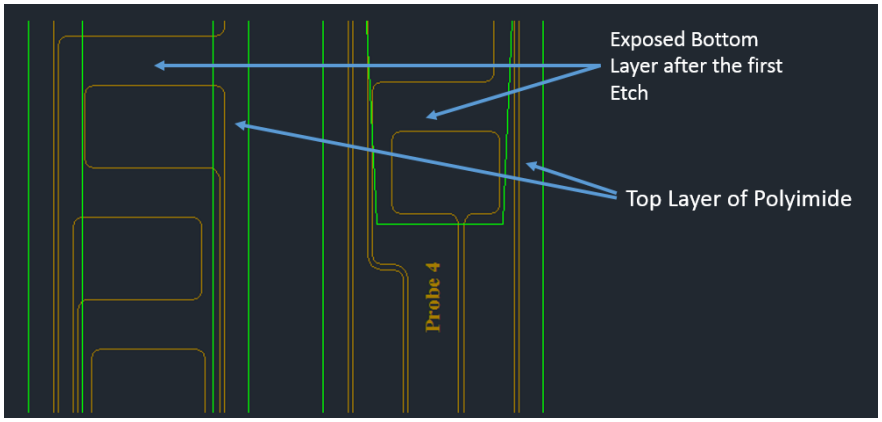

Figure 2.8: AutoCAD models of the Mask showing the exposed bottom layer of PI, after the top layer etch

was large and disturbed the impedance measurements.

This led us to the final recipe, where the top layer of polyimide opened up the bond pads and sensor region, just enough for their functionality. This prevented the exposure of the bottom polyimide layer around the conductive region. This method also eliminated one step of titanium deposition and its subsequent patterning. Figure 2.9 shows the change in the

mask that doesn't leave a gap to expose the bottom polyimide layer.

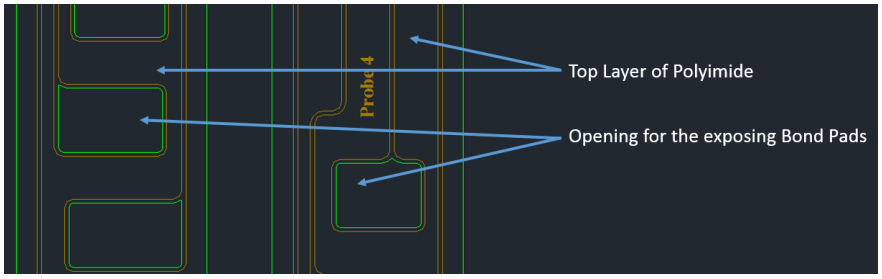

Figure 2.9: Changed mask that doesnt expose the bottom PI layer.

The change in the recipe improved the overall yield, and the final devices were sturdy. Scanning Electron Microscope images of the probe shows a sharp step etch of the top layer of polyimide, with no undercutting or visible defects. Figures 2.11a, 2.11b and 2.12 shows the SEM images of the probe, imaged at the sections marked in red in figures 2.10a and 2.10b. The SEM image in figure 2.11a has a magnification of 3000X and the figure 2.11b has a magnification of 25,000X. The images were taken with a tilt of 35°to observe the depth between the top layer of Polyimide and the gold bond pad

The final recipe that is optimized for the fabrication of the probes is enlisted in Appendix and is schematically presented in the figure 2.13 below.

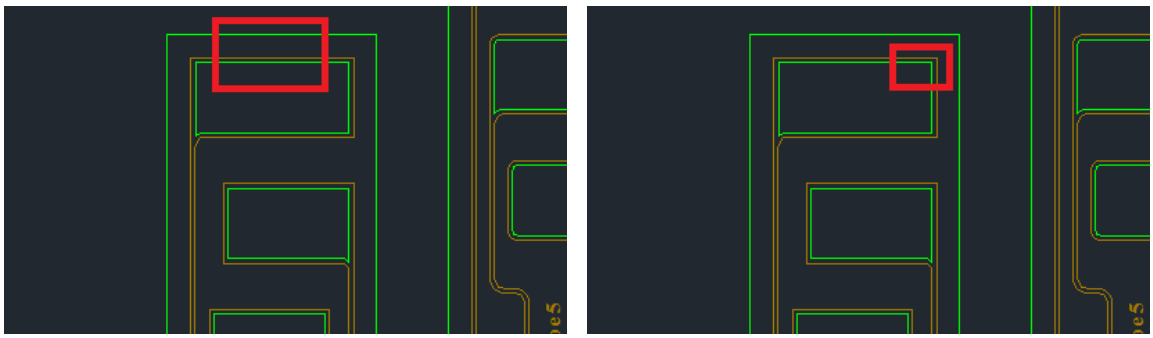

(a) Position 1 (b) Position 2

Figure 2.10: Schematic of the location of the scan on the probe is marked by the red square.

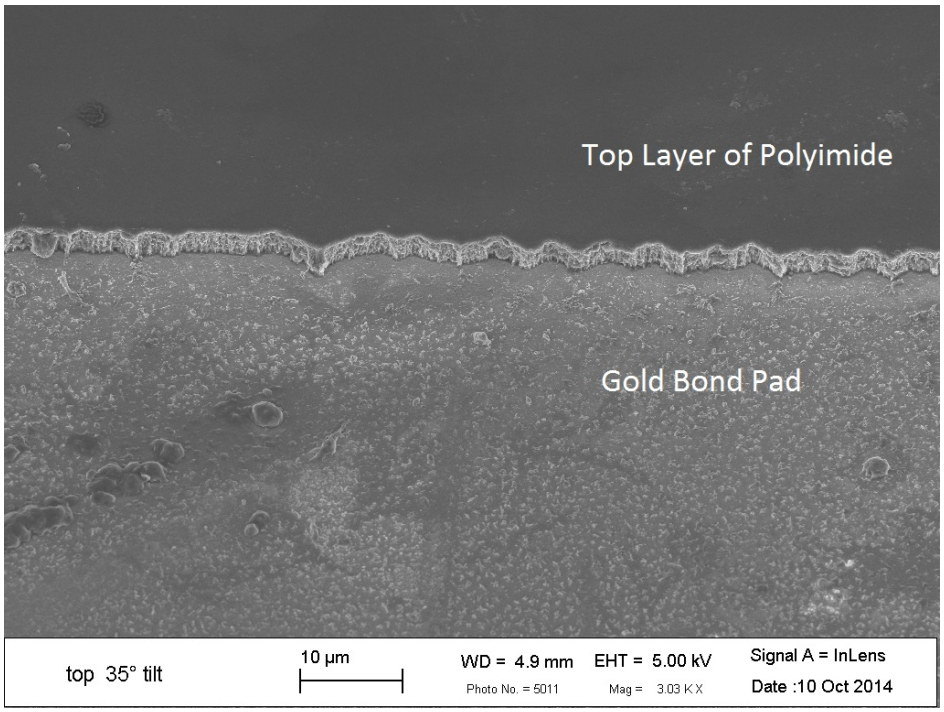

(a) Zoom of 3kX

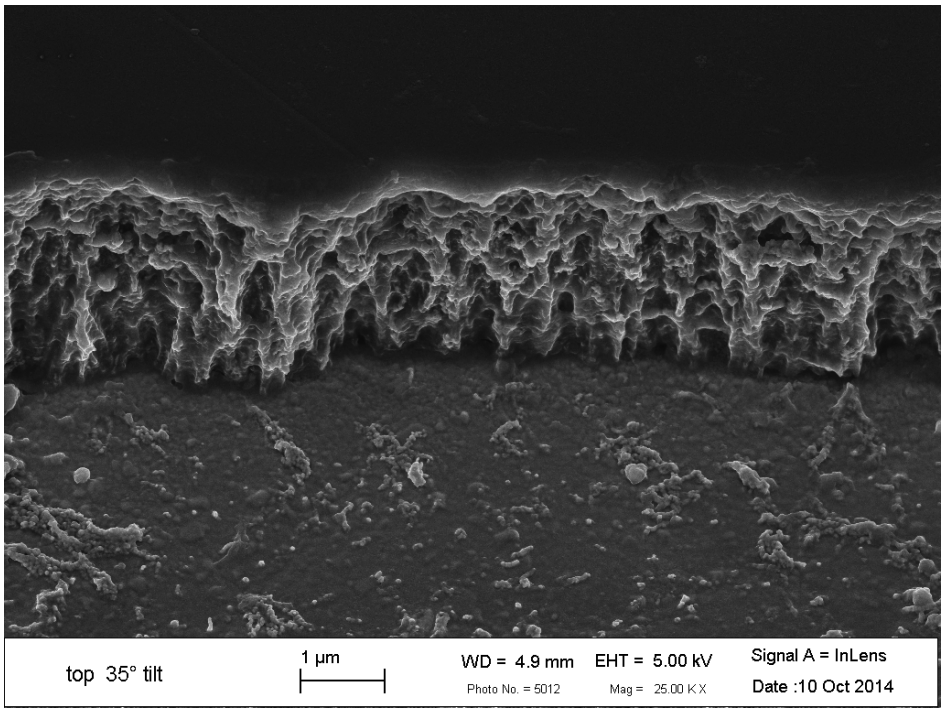

(b) Zoom of 25kX

Figure 2.11: SEM images of the probe at position indicated in figure 2.10a

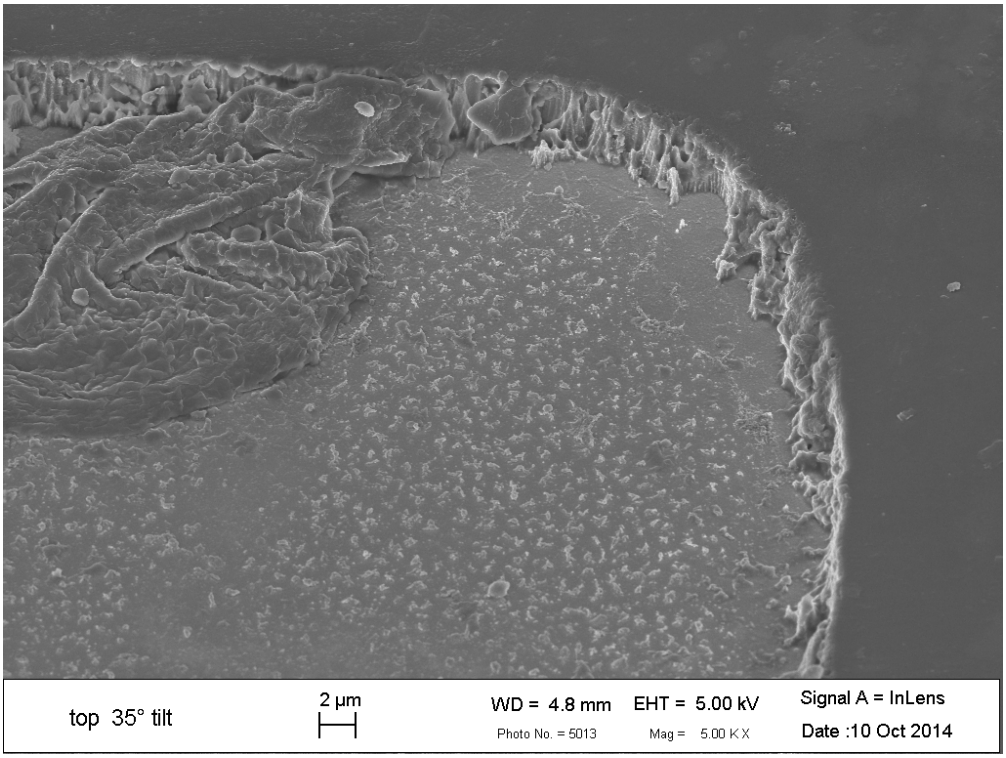

Figure 2.12: Scanning Electron Microscopy images of the probe at magnification of 5kX and at the position indicated in the figure 2.10b

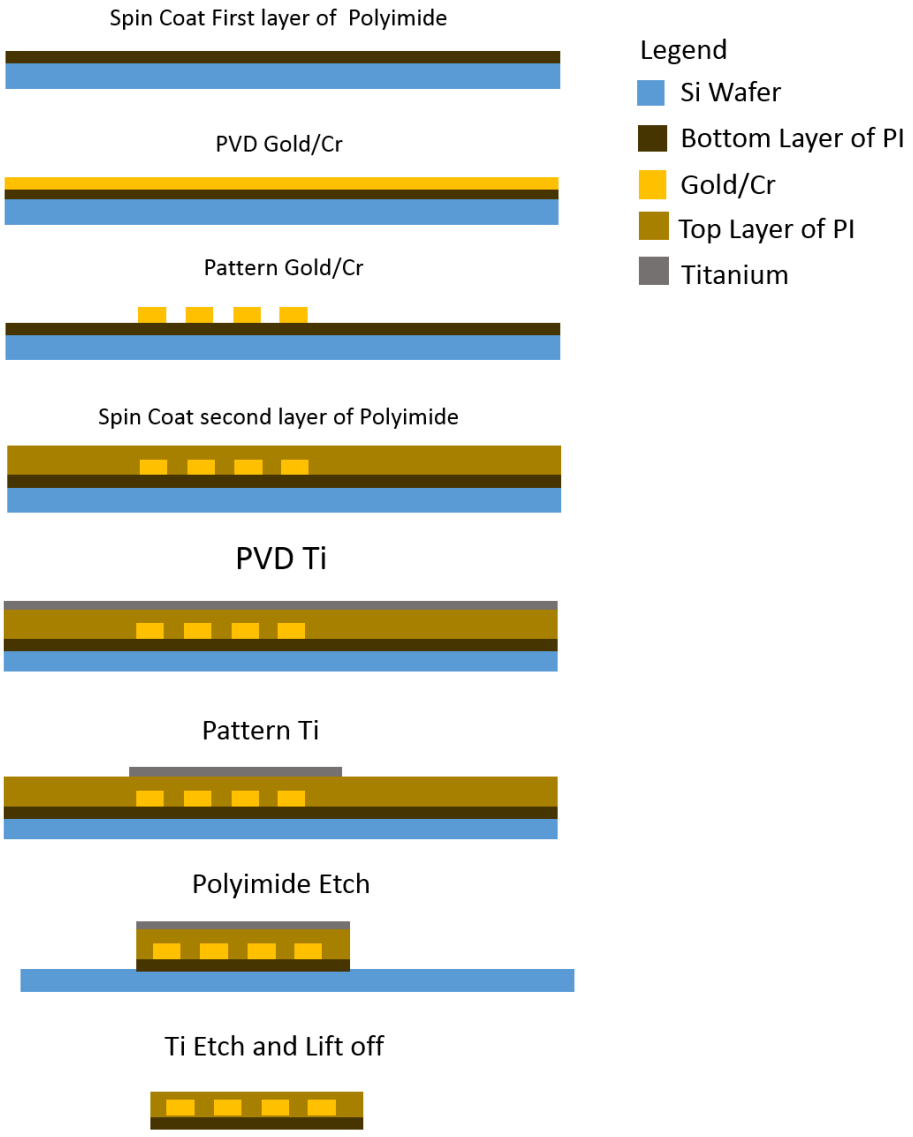

Figure 2.13: Schematic of the final recipe for fabricating these structures.

Chapter 3

Calibration and Results

The fabricated probes were then mounted on a firm surface, like a biopsy needle or a flat diced wafer. Wires were carefully bonded using medium temperature solder (<700F), as is the common practice, epoxy resins or glues were molded along the bond pads. This firmly holds the solder and distributes any stress on the solder bond pad to the rest of the probe. Figure 3.1a shows a probe which is mounted on a diced wafer and ready for calibration and testing. Figure 3.1b shows the fabricated probe on a mounted on a catheter using epoxy glue, and ready for further calibration

The previous chapter dealt in detail with the design criteria that would impact the cell constant 'κ' of any probe. The two electrode probes are mostly discouraged for measuring any anisotrpic media mainly because the following assumption, which is important to estimate cell constant doesn't hold

$$RC = \frac{\epsilon_0 \epsilon_r}{\sigma} \tag{3.1}$$

Thus we use the fabricated four electrode probes for measurement.

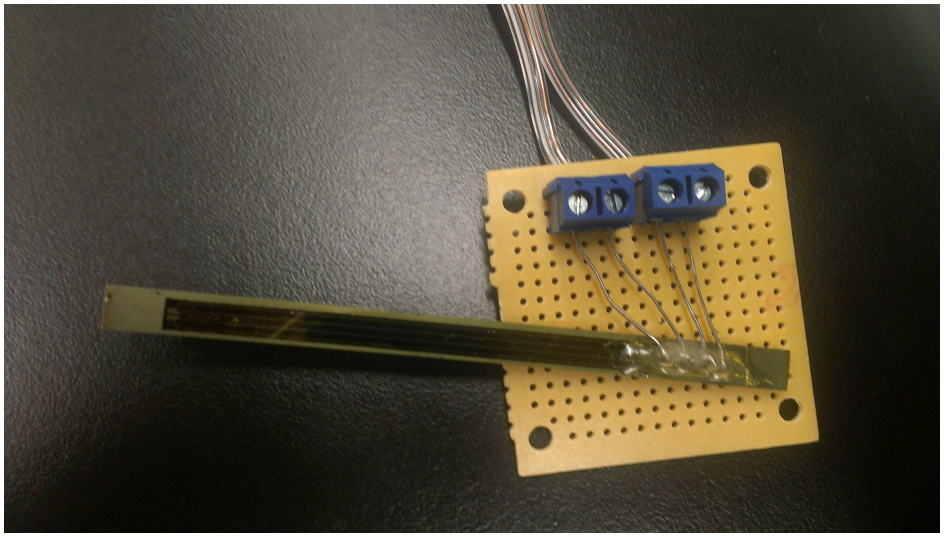

(a) Device on a Diced Wafer

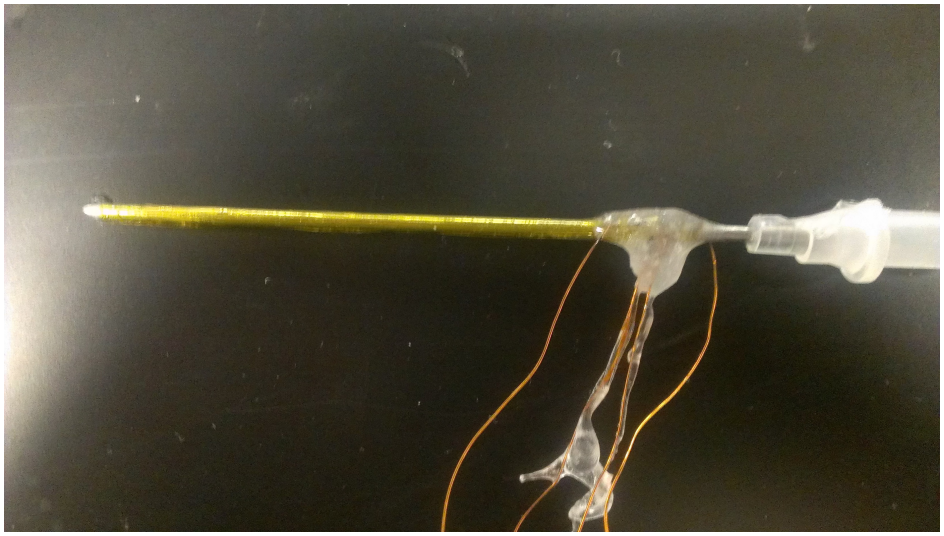

(b) Device on a Biopsy catheter

Figure 3.1: Bonded Electrode Probes ready for calibration

3.1 Calibration of the Probes

While there are substantial theoretical methods to estimate the cell constant of a four-electrode probe, it is easier and more accurate to determine the cell constant experimentally. The impedance of the probe is calculated using the formula below

$$R = \frac{V_{measured}}{I_{applied}} \tag{3.2}$$

where '$V_{measured}$' is the voltage drop across the inner electrodes of the probe and measured using an oscilloscope (Textronix DPO 2012), and 'I_{input}' is the current input to the outer electrodes of the probe. Signal generator—Agilent 33120A—was used to supply AC voltage and the current input to the probe was measured by measuring the voltage drop across a known resistor. The following circuit, shown in figure 3.2, was used to evaluate the probe's impedance readings

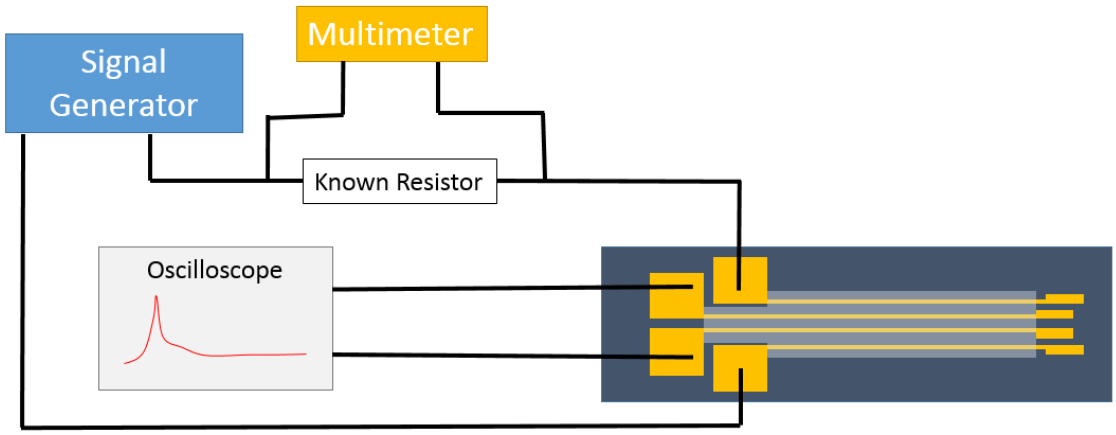

Figure 3.2: Schematic of the circuit used for probe calibration

For most calibration runs, the signal generated was 1VPP and 20 kHz. Theoretically, the

impedance measured from these probes is frequency independent at higher frequencies. This is the region where the effects from stray capacitances are minimum. To understand how the probe reacts at various frequencies, an impedance spectroscopy of the device in 1% salt solution was measured using the Potentiostat Experiment in Gamry Impedance Analyzer. Figure 3.3, shows the results of that experiment. From the graph below, it can be observed that the impedance measured remains substantially flat between 1 kHz–1 MHz

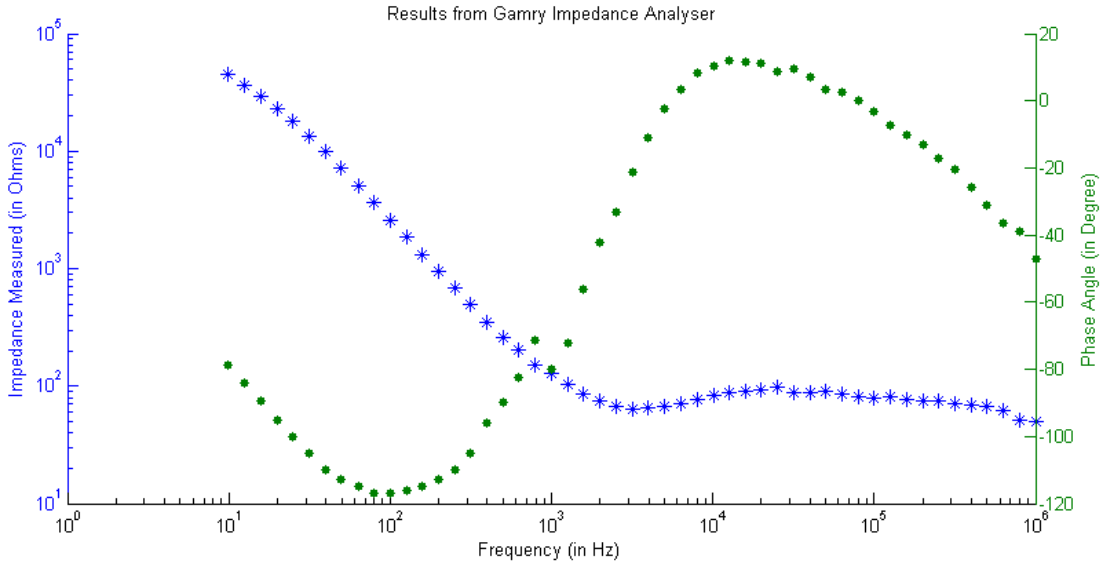

Figure 3.3: Impedance spectroscopy of a 4-electrode probe using Gamry Impedance Analyser

Figure 3.4, are calibration curves obtained for two different probes for a signal of 1VPP and at 20 kHz. The probes used where Probe 5 (3^{rd} from left) and Probe 6 (2^{nd} from left) as marked in figure 2.5

The salt solutions used were prepared using lab grade 99.9% NaCl salt, titrated over DI water. The conductivity of the solution was carefully measured using a four-electrode commercial impedance measurement probe and was also subsequently compared against the published values of impedivity for particular percentage of weight salt solution.

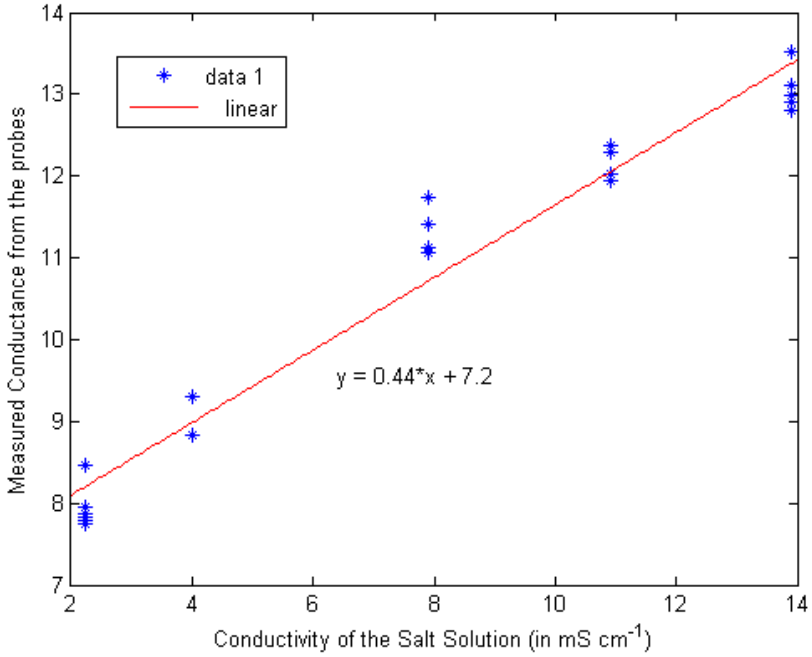

(a) Probe 5

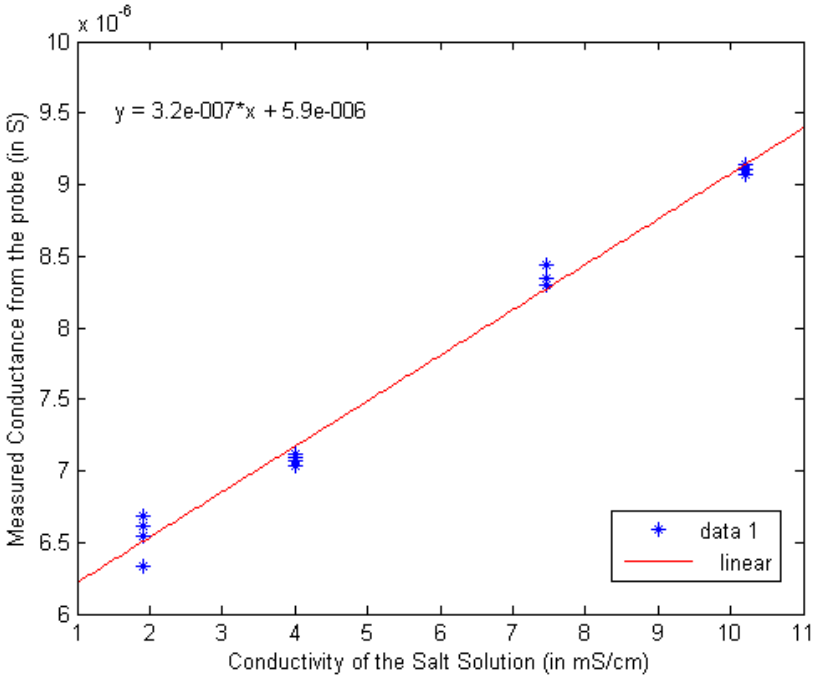

(b) Probe 6

Figure 3.4: Calibration Results of the probes

3.2 Ex-Vivo Porcine Tissue

With the calibrated probes, it was now possible to measure conductivities of any given media. Conductivities of porcine tissues where measured and compared against published literature. The ex-vivo measurements where done on porcine kidneys and livers between 4–8 hours, for every hour, after the euthanization. Typically the animal was euthanized at 0730 HRS and the first measurement was done at 1130Hrs, and the experiment continued till 1535 Hrs.

The measurements where done using the calibrated probe-6, which rested on the silicon wafer. Prior to the insertion of the probes, small cuts on the organs of approximately 1–2cm wide and 1 cm deep was done using a typical scalpel. The cuts were equally spaced on the organs—three cuts in every lobe of the liver, and six cuts in the kidney, with 2 each at the top, middle, and bottom. Figures 3.5a and 3.5b shows the cuts in yellow circles. Subsequently, the probes were inserted and the conductance value was measured using the same circuit described for their calibration. Figure 3.6 shows the conductance measurement done on the porcine liver

The measurements where done using a 1V peak-to-peak sinusoidal signal at 100 kHz. Gabriel et al [27] demonstrated that the tissue conductivity of a porcine liver was between 0.075 S/m-0.2 S/m. Table 3.1 shows the measured conductivity for various times during the experiment

To the best of our knowledge there is no literature that measures the conductivity of porcine kidney exactly at 100kHz, the seminal on tissue dielectric properties by Gabriel et al [28] demonstrates that the conductivity of most animal kidney tissue is between 0.1S/m–0.35 S/m. Table 3.2 lists the results of the measured conductance of porcine kidney at various times since euthanization. It can be observed that the values lie within the range of measurements indicated in [28].

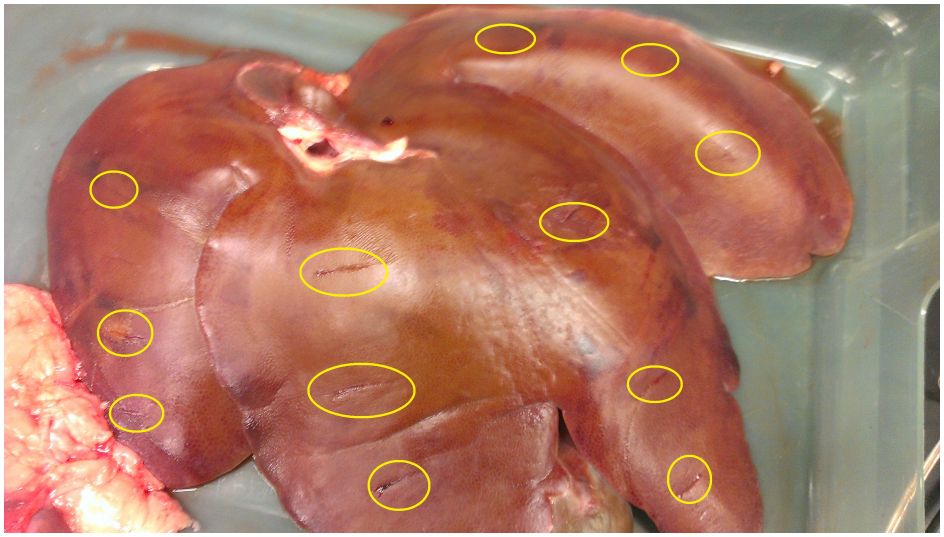

(a) Porcine Liver

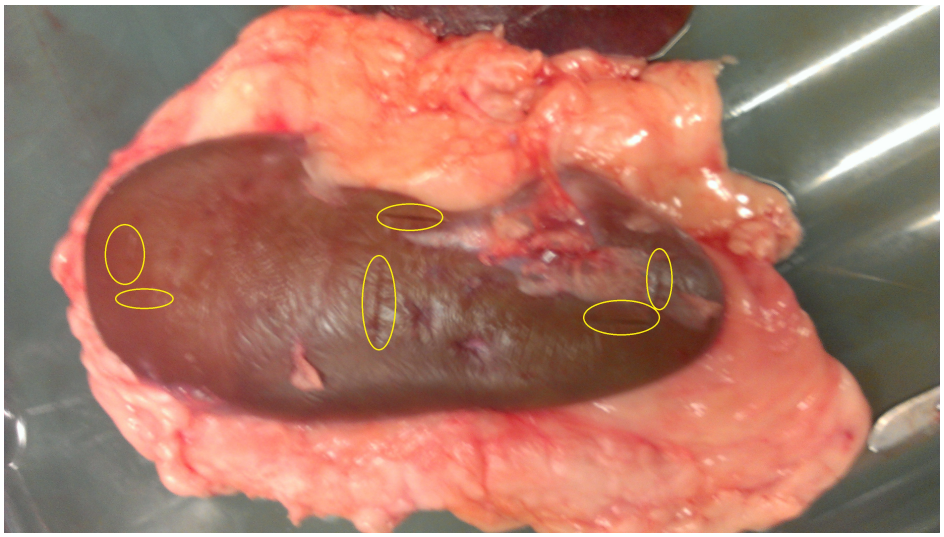

(b) Porcine Kidney

Figure 3.5: Porcine tissues for conductivity measurements using the fabricated probes. Yellow circles denote the area where the measurement was done.

Table 3.1: Conductivity measurements of porcine liver

Time since euthanization (in Hrs)	Measured Conductivity (in S/m)
4	0.121
5	0.106
6	0.110
7	0.113
8	0.113

Table 3.2: Conductivity measurements of porcine kidney

Time since euthanization (in Hrs)	Measured Conductivity (in S/m)
4	0.193
5	0.202
6	0.162
7	0.186
8	0.182

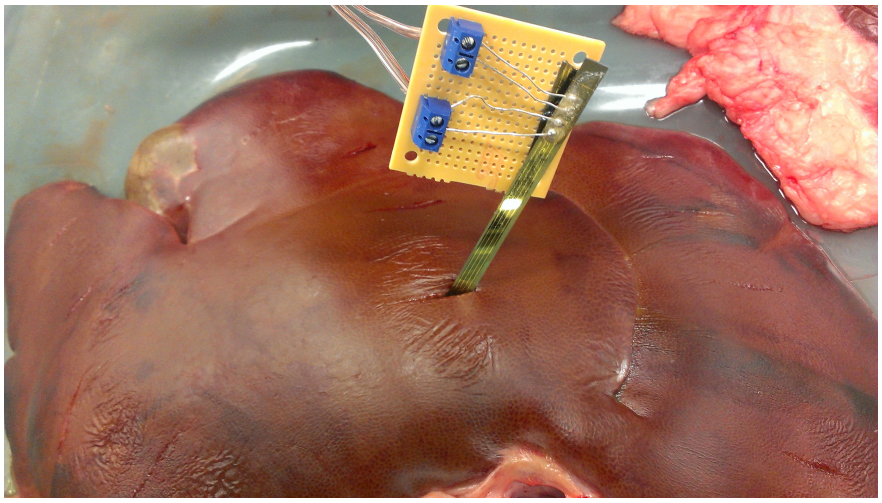

Figure 3.6: Conductance measurement experiment done on the porcine liver

3.3 Results of Stacked Agar Phantoms

While we have demonstrated that the probe is calibrated and can measure with a fair accuracy the conductivities of tissue, the probes are, however, designed to estimate with a fairly small spatial resolution the interface of two different conductive media. In this section we mimic the changing conductivity at the tissue-tumor interface with agar phantoms of different conductivities stacked over the other, and use our probe to identify this interface.

The agar phantoms were prepared by heating 10gm of agar, 6gm of sucrose and 2gm of NaCl in 200 ml of deionized water. The conductivity of the gel can be manipulated by changing the amount of NaCl used [29]. The first agar phantom, '**A**', which was prepared with 0.01 gm of NaCl, had a conductivity of 1.15mS/cm when measured using commercial impedance measurement probe. The second agar phantom, '**B**', which was prepared using 1gm of NaCl had a higher conductivity of 15.3 mS/cm, as measured by the commercial probe. The agar phantom '**A**' was approximately 18mm thick while the agar phantom '**B**' was 40mm thick. The schematic of the experimental setup is as shown in figure 3.7. The probe was now inserted and the measured impedance was noted for every step. The reading was done three times at every step to monitor any drifts. Effective conductivity measured can be calculated

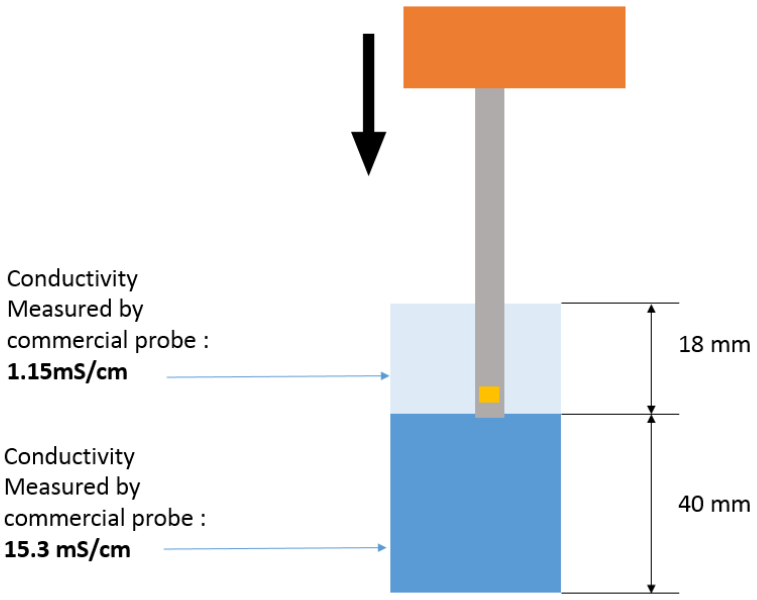

Figure 3.7: Sketch of the experimental set-up

using the cell constant obtained in the calibration. With this technique the interface of the two agar phantoms was identified. The measured conductivity values from the probes correspond closely with the measurements obtained using the commercial electrodes.

Figure 3.8 plots the impedance against distance, and the shaded region is the identified interface. The observed interface could lie anywhere between ∼13mm–17mm, demonstrating a spatial resolution of ∼4mm. The dimensions of the probe used is shown in figure 3.9. From the theoretical predictions described in section 2.2 and from the figure 2.4, the spatial resolution to identify the interface was estimated to be 4 times the inter-electrode distance 'a'. The probe used for these measurements had an inter-electrode distance of 500µm. Thus the theoretical estimation of the spatial resolution was 2mm.

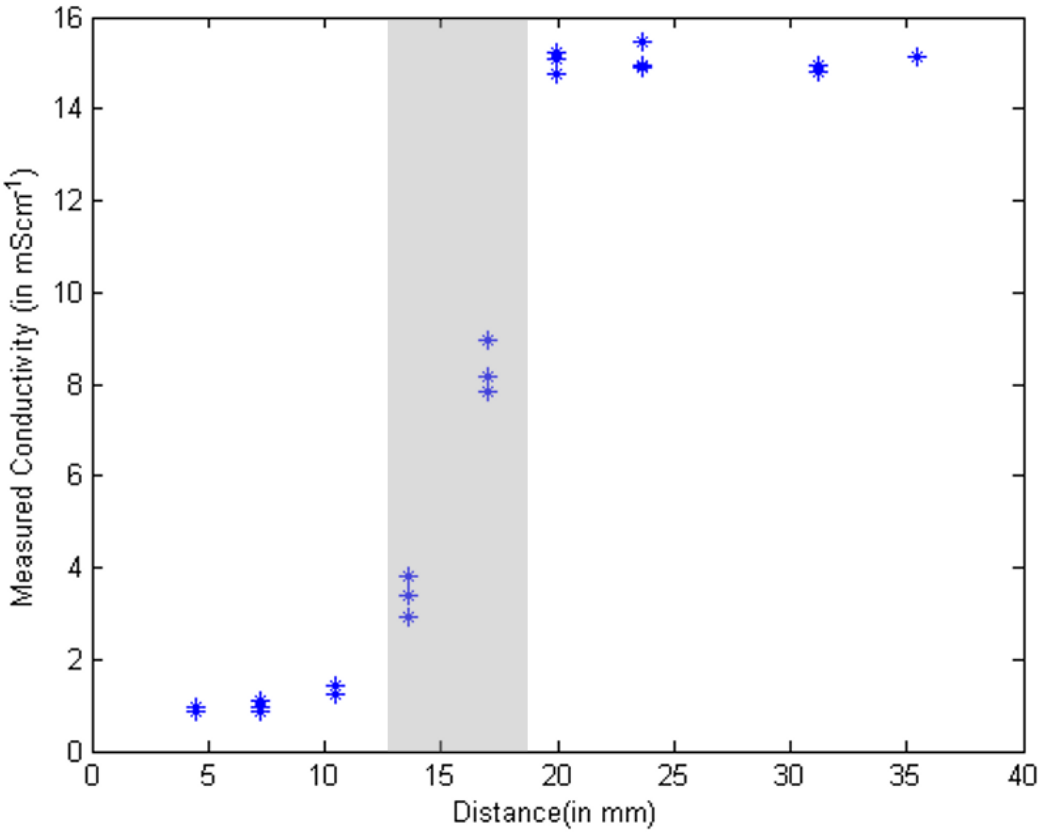

Figure 3.8: Measured conductivity of the stacked agar gels using the 4-electrode probe

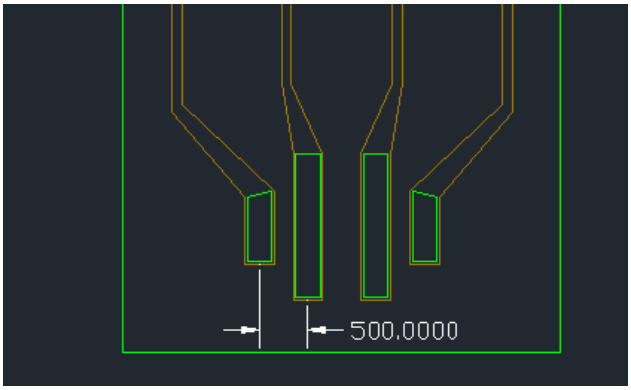

Figure 3.9: Inter-electrode distance of the probe used is 500μm

Chapter 4

Conclusions and Future Work

4.1 Conclusion

This thesis established the need to mitigate the problem of cancer cell seeding during biopsy procedures, and described the development of a smart biopsy tool to address this problem. The work focused on development of the bio-impedance measurement sensor which is an integral part of the smart biopsy tool.

The bio-impedance sensor was built using conventional MEMS fabrication techniques by sandwiching conductive gold electrodes between insulating polyimide thin films. These sensors, once fabricated, can be integrated with the biopsy tool. The sensors were further characterized with known salt solutions to estimate the cell-constant of the device.

These sensors were tested against a specially prepared agar phantoms which have conductivities similar to those of regular and malignant tissue. The exact position of the interface of the agar phantoms with different conductivity was measured using the developed bio-impedance sensor.

In this work we have zeroed-in on a fabrication recipe, with which these sensors can be developed, and we, now, have a sensor, which yields fairly accurate and linear response to changing media conductivities. This sensor can be easily mounted on a biopsy needle without affecting its functionality. With simple electronics, the tissue conductivity can be monitored during the procedure.

4.2 Future work

While the sensing component of the 'smart-biopsy' tool is ready, substantial work needs to be done before the dream of biopsies without the risk of cancer cell dissemination is achieved.

The RF sleeve needs to be now fabricated, tested and optimized for the specific purpose. With integration of this sleeve, it is important that the tools efficacy is measured by testing under lab conditions, using mice with highly differentiated tumors, and compare the results with the studies posted by Ryd et al [4]. This will provide a basis to quantify the reduction in the risk of these procedures.

Other possible complications while using this procedure needs to be identified. To commercialize this device for usage under hospital conditions it is important to develop electronics that can be used by personnel with little skill. Combining the signal generator and the voltmeter to give a simple impedance reading will help practicing physicians with little engineering knowledge to use the device. It will be a wholesome product if the electronics of the RF sleeve component can be combined with the electronics of the sensor, and the tool be made modular.

Bibliography

[1] E. H. Smith, "The hazards of fine-needle aspiration biopsy," *Ultrasound in medicine & biology*, vol. 10, no. 5, pp. 629–634, 1984.

[2] R. Terry, "Risks of needle biopsy of the liver," *British medical journal*, vol. 1, no. 4768, p. 1102, 1952.

[3] T. Livraghi, B. Damascelli, C. Lombardi, and I. Spagnoli, "Risk in fineneedle abdominal biopsy," *Journal of Clinical Ultrasound*, vol. 11, no. 2, pp. 77–81, 1983.

[4] W. Ryd, B. Hagmar, and O. Eriksson, "Local tumour cell seeding by fineneedle aspiration biopsy," *Acta Pathologica Microbiologica Scandinavica Series A: Pathology*, vol. 91, no. 16, pp. 17–21, 1983.

[5] E. Robertson and G. Baxter, "Tumour seeding following percutaneous needle biopsy: The real story!," *Clinical radiology*, vol. 66, no. 11, pp. 1007–1014, 2011.

[6] E. H. Smith, "Complications of percutaneous abdominal fine-needle biopsy. review.," *Radiology*, vol. 178, no. 1, pp. 253–258, 1991.

[7] M. A. Silva, B. Hegab, C. Hyde, B. Guo, J. A. Buckels, and D. F. Mirza, "Needle track seeding following biopsy of liver lesions in the diagnosis of hepatocellular cancer: a systematic review and meta-analysis," *Gut*, vol. 57, no. 11, pp. 1592–1596, 2008.

[8] C. Boutin, F. Rey, and J.-R. Viallat, "Prevention of malignant seeding after invasive diagnostic procedures in patients with pleural mesothelioma a randomized trial of local radiotherapy," *CHEST Journal*, vol. 108, no. 3, pp. 754–758, 1995.

[9] R. Knight, K. Horiuchi, S. H. Parker, E. R. Ratzer, and M. E. Fenoglio, "Risk of needle-track seeding after diagnostic image-guided core needle biopsy in breast cancer," *JSLS: Journal of the Society of Laparoendoscopic Surgeons*, vol. 6, no. 3, p. 207, 2002.

[10] J. Woitzik and J. Krauss, "Polyethylene sheath device to reduce tumor cell seeding along the needle tract in percutaneous biopsy," *Surgical Endoscopy And Other Interventional Techniques*, vol. 17, no. 2, pp. 311–314, 2003.

[11] A. Ivorra, "Electrochemical prevention of needle-tract seeding," *Annals of biomedical engineering*, vol. 39, no. 7, pp. 2080–2089, 2011.

[12] F. Mu, S.-P. Liu, X.-L. Zhou, J.-B. Chen, H.-B. Li, J.-S. Zuo, and K.-C. Xu, "Prevention of needle-tract seeding by two-step freezing after lung cancer biopsy," *Pathology & Oncology Research*, vol. 19, no. 3, pp. 447–450, 2013.

[13] Z. Liu, M. Ahmed, Y. Weinstein, M. Yi, R. L. Mahajan, and S. N. Goldberg, "Characterization of the rf ablation-induced 'oven effect': The importance of background tissue thermal conductivity on tissue heating," *International journal of hyperthermia*, vol. 22, no. 4, pp. 327–342, 2006.

[14] H. Fricke and S. Morse, "The electric capacity of tumors of the breast," *The Journal of Cancer Research*, vol. 10, no. 3, pp. 340–376, 1926.

[15] S. R. Smith, K. Foster, and G. L. Wolf, "Dielectric properties of vx-2 carcinoma versus normal liver tissue," *Biomedical Engineering, IEEE Transactions on*, no. 5, pp. 522–524, 1986.

[16] K. Foster and J. Schepps, "Dielectric properties of tumor and normal tissues at radio through microwave frequencies," *The Journal of microwave power*, vol. 16, no. 2, pp. 107–119, 1981.

[17] T. Morimoto, S. Kimura, Y. Konishi, K. Komaki, T. Uyama, Y. Monden, D. Y. Kinouchi, and D. T. Iritani, "A study of the electrical bio-impedance of tumors," *Investigative Surgery*, vol. 6, no. 1, pp. 25–32, 1993.

[18] D. Haemmerich, S. Staelin, J. Tsai, S. Tungjitkusolmun, D. Mahvi, and J. Webster, "In vivo electrical conductivity of hepatic tumours," *Physiological measurement*, vol. 24, no. 2, p. 251, 2003.

[19] R. Davalos and B. Rubinsky, "Electrical impedance tomography of cell viability in tissue with application to cryosurgery," *TRANSACTIONS-AMERICAN SOCIETY OF MECHANICAL ENGINEERS JOURNAL OF BIOMECHANICAL ENGINEERING*, vol. 126, no. 2, pp. 305–308, 2004.

[20] R. V. Davalos, D. M. Otten, L. M. Mir, and B. Rubinsky, "Electrical impedance tomography for imaging tissue electroporation," *Biomedical Engineering, IEEE Transactions on*, vol. 51, no. 5, pp. 761–767, 2004.

[21] A. Nussbaum, *Electromagnetic theory for engineers and scientists*. Prentice-Hall, 1965.

[22] K. H. R and P. S. Castro, "Capacitance between thin film conductors deposited on a high dielectric-constant substrate," *Proc. IRE (Corresp.)*, vol. 50, pp. 2142–2143, 1962.

[23] P. Steendijk, G. Mur, E. T. Van Der Velde, and J. Baan, "The four-electrode resistivity technique in anisotropic media: theoretical analysis and application on myocardial tissue in vivo," *Biomedical Engineering, IEEE Transactions on*, vol. 40, no. 11, pp. 1138–1148, 1993.

[24] M. F. Suesserman and F. A. Spelman, "Quantitative in vivo measurements of inner ear tissue resistivities. i. in vitro characterization," *Biomedical Engineering, IEEE Transactions on*, vol. 40, no. 10, pp. 1032–1047, 1993.

[25] A. Ivorra, R. Gomez, N. Noguera, R. Villa, A. Sola, L. Palacios, G. Hotter, and J. Aguilo, "Minimally invasive silicon probe for electrical impedance measurements in small animals," *Biosensors and bioelectronics*, vol. 19, no. 4, pp. 391–399, 2003.

[26] P. N. Robillard and D. Poussart, "Spatial resolution of four electrode array," *Biomedical Engineering, IEEE Transactions on*, no. 8, pp. 465–470, 1979.

[27] C. Gabriel, A. Peyman, and E. Grant, "Electrical conductivity of tissue at frequencies below 1 mhz," *Physics in medicine and biology*, vol. 54, no. 16, p. 4863, 2009.

[28] C. Gabriel, "Compilation of the dielectric properties of body tissues at rf and microwave frequencies," report, DTIC Document, 1996.

[29] M. Yi, H. V. Panchawagh, R. L. Mahajan, Z. Liu, and S. N. Goldberg, "Micromachined electrical conductivity probe for rf ablation of tumors," in *ASME 2005 International Mechanical Engineering Congress and Exposition*, pp. 53–56, American Society of Mechanical Engineers.

Appendix

A Recipe for Device Fabrication

Step 1 IPA Clean of Si Wafer.

Step 2 Prepare adhesion promotoer for PI-2525, by diluting 1ml of VM651 in 1L of DI-water

Step 3 Carefully apply the adhesion promoter along the edges of the wafer. Heat it at 110°C for 90 seconds.

Step 4 Spin Coat PI-2525 at 500RPM for 10 secs and at 3000 RPM for 40 secs

Step 5 Softbake the wafer on a hot plate at 110°C for 3 minutes.

Step 6 PVD Gold/Chrome on the wafer. Final thickness of Gold sputtered is 500Å–800Å

Step 7 Spin coat PR AZ9260 at 2000 RPM, and softbake at 110°C for 1 minute.

Step 8 Pattern the PR using Mask 1

Step 9 With PR as the mask etch Gold and Chrome in their respective etchants

Step 10 Once etched, remove the PR from the wafer using a subsequent IPA clean.

Step 11 Apply the adhesion promoter throughout the wafer and spin it dry.

Step 12 Heat the wafer dry for 30 secs at 110°C

Step 13 Spin Coat the second PI layer at 500 RPM for 10 secs and 5000 RPM for 40 secs

Step 14 Softbake for over a minute on a hot plate at 110°C

Step 15 The wafer is ready for hard baking. Introduce the wafers in the oven and slowly ramp the temperature to 200°C. Use a ramp rate of 5°C/min.

Step 16 Hold at 200°C for 30 mins

Step 17 Introduce Nitrogen atmosphere, by using Nitrogen flow typically at 10L/min

Step 18 Ramp the temperature to 300°C using a ramp rate of 5°C/min.

Step 19 Hold at 300°C for 30 mins.

Step 20 Bring the wafer to room temperature using a ramp of 5°C/min.

Step 21 PVD Titanium. Deposit not more the 1.2KÅ of the metal.

Step 22 Pattern titanium using PR AZ9260, and subsequent etch in BOE 6:1 for less than a minute at room temperature.

Step 23 Strip the PR mask using IPA clean

Step 24 With Ti as mask etch PI layers in Oxygen plasma for approximately 75 minutes. Intermittently check for the etch rates. Use a max power of 50 Watts.

Step 25 Once the bottom PI is also etched. Introduce the wafer in BOE 6:1 for about a minute. Ti mask will be stripped and the probes will be released during this procedure. Carefully remove the probes using protective gear and wash them profusely in DI water to remove any BOE adhering on them